Streaks in high-speed boundary layers: assessment via the full nonlinear boundary-region equations

Adrian Sescu*[1], Mohammed Afsar†[2], and Yuji Hattori‡[3]

[1]Department of Aerospace Engineering, Mississippi State University, MS 39762
[2]Department of Mechanical & Aerospace Engineering, Strathclyde University, 75 Montrose St. Glasgow, G1 1XJ, UK
[3]Institute of Fluid Science, Tohoku University, 2 Chome-1-1 Katahira, Aoba Ward, Sendai, 980-8577, Japan

Streamwise vortices and the associated streaks evolve in boundary layers over flat or concave surfaces as a result of various disturbances initiated in the upstream or from the wall surface. Following the transient growth phase, the fully-developed vortex structures become susceptible to inviscid secondary instabilities resulting in early transition to turbulence via bursting processes. In the incompressible regime, a vast body of work has been devoted to understand the initiation and development of these streaks, as well as the conditions under which they undergo secondary instabilities. For high-speed boundary layers, on the other hand, additional complications due to the compressibility and thermal effects arise, the level of contribution of which scales with the Mach number. In this paper, we study streaks in high-speed boundary layers via the numerical solution to the full nonlinear boundary region equations, which is the high Reynolds number asymptotic form of the Navier-Stokes equations, under the assumption that the streamwise wavenumber of the disturbances is much smaller than the wavenumbers associated with the crossflow directions, commensurate with long streamwise wavelength of the primary vortex disturbance. The effect of the spanwise separation of the vortices and the Mach number, which is varied between high-subsonic ($M = 0.8$) to low-hypersonic ($M = 6$) regimes, is quantified and discussed.

I. Introduction

Streaks formation in pre-transitional boundary layer flows over flat or curved surfaces occur when the height of roughness elements exceeds a certain critical value (e.g., Choudhari & Fischer,[2] White,[41] White et al.,[42] Goldstein et al.,[6–8] or Wu & Choudhari[43]), or the amplitude of the free-stream disturbances is greater than a given threshold (e.g., Kendall,[16] Westin et al.,[40] Matsubara & Alfredsson,[25] Leib et al.,[18] Zaki & Durbin,[47] Goldstein & Sescu,[9] or Ricco et al.[29]). The stream-wise component of velocity exhibit elongated 'streaky' features, characterized by adjacent regions of acceleration (high-speed) and deceleration (low-speed) of fluid particles (e.g., Kendall,[16] Matsubara & Alfredsson,[25] or Landahl[17]). Elongated streaks in the form of stream-wise (Görtler) vortices also appear inside a boundary layer flow along a concave surface due to the imbalance between radial pressure gradients posed by the wall, and centrifugal forces (e.g., Gortler,[10] Hall,[12–14] Swearingen & Blackwelder,[37] Malik & Hussaini,[23] Saric,[32] Li & Malik,[19] Boiko et al.,[1] Wu et al.,[44] or Sescu et al.,[34,35] Ren & Fu,[27] Dempsey et al.,[3] Xu et al.[45]). For highly curved walls, for example, vortex formation occurs more rapidly and can significantly alter the mean flow causing the laminar flow to breakdown into turbulence. Under certain conditions, however, Görtler vortices can be efficient precursors to transition: i.e., they consist of counter-rotating streamwise vortices that grow at a certain rate, depending on the surface curvature and the receptivity of the boundary layer to environmental

*Associate Professor, Department of Aerospace Engineering, Mississippi State University; Associate Fellow AIAA.
†Chancellor Fellow, Department of Mechanical & Aerospace Engineering; AIAA member.
‡Professor, Institute of Fluid Science, Tohoku University.

disturbances and surface imperfections. In boundary layers over surfaces having small to medium curvature, these vortices can significantly alter the mean flow and cause the laminar flow to breakdown.

It was recognized in many studies that boundary layer streaks are important in the path of transition to turbulence in a laminar flow. Many previous studies and results indicated that it is the transient part of the disturbance that dominates the growth of streaks or other three-dimensional disturbances that lead to breakdown, so any effective method of control must focus on restricting the development of the transient modes.

In the compressible regime, streak development under different scenarios, such as bypass transition or flows over concave surfaces, remains largely unexplored. A number of experiments have been conducted to establish the gross correlation between the transition Reynolds number and freestream turbulence (FST) level. They showed that the transition position shifts significantly depending on both FST level (Dryden,[4] Schneider[36]) and surface roughness (e.g. Pate[26]). However, there exist only a few investigations of the detailed physics underlying such correlation. The experiments of Kendall[15] provide much information concerning supersonic boundary-layer transition under the influence of high level of FST. A salient feature is that fluctuations over a wide frequency range undergo substantial growth within the boundary layer. Sufficiently downstream, a spectral peak emerges, which corresponds to the Mack-I mode in the low-Mach-number supersonic range (M $<$ 4.5) (Mack[22]). For higher Mach numbers, a secondary, less pronounced peak representing the Mack-II instability was observed to appear. These results indicate that some kind of receptivity mechanism operates to generate instability waves in a nominally flat plate. Ricco & Wu[29] extended the incompressible analysis by Leib et al.[18] to the compressible case and explained the formation and growth of thermal streaks, which are thought to play a significant role in the secondary instability process. Ricco, Tran & Ye[31] and Ricco, Shah & Hicks[30] further studied the influence of wall heat transfer and wall suction, respectively, on the thermal streaks.

The focus of the present paper is on the investigation of streamwise vortices and the associated streaks that develop in high-speed boundary layers over concave surfaces by using the full nonlinear boundary region equations. The latter set of equations form the high Reynolds number asymptotic limit of the Navier-Stokes equations under the assumption that the streamwise wavenumber of the disturbances is much smaller than the wavenumbers associated with the crossflow directions as in the incompressible case. This set of equations is parabolic in the streamwise direction, allowing for a straightforward marching procedure to be applied along the streamwise direction. To this end, upstream or initial conditions have to be imposed to start the calculation, which is accomplished via a set of initial conditions that were previously derived by Ricco.[28] Since a concave wall is considered in the analysis, the disturbances take the form of Görtler instabilities, featuring counter rotating pairs of vortices and associated streaks that resemble mushroom shapes in contours of streamwise velocity plotted in crossflow sections. We analyze and quantify the evolution of these streaks via contour plots of temperature in crossflow planes, as well as vortex energy, wall shear stress, or wall heat flow distributions versus the streamwise coordinate.

In section II, the mathematical model is introduced and described. Here we discuss the scalings of various independent or dependent variables, the appropriate initial and boundary conditions, as well as the numerical algorithm. In section III, results for various freestream Mach numbers and spanwise separation, in high-subsonic, supersonic and low-hypersonic regimes are reported and discussed. Concluding remarks are included in the last section IV.

II. Problem formulation and numerical algorithm

We consider a compressible flow of uniform velocity V_∞^* and temperature T_∞^* past a flat or curved surface. The air is treated as a perfect gas such that the sound speed in the free-stream $c_\infty^* = \sqrt{\gamma R T_\infty^*}$, where $\gamma = 1.4$ is the ratio of the specific heats, and $R = 287.05 Nm/(kgK)$ is the universal gas constant; Mach number is assumed to be of order one. The flow is divided into four regions as in Leib et al.,[18] Ricco & Wu[29] or Marensi et al.[24] (see figure 1):

- Region I is in proximity to the the leading edge, outside of the boundary layer, where the flow is assumed inviscid and the disturbances are treated as small perturbations of the base flow.
- Region II is the boundary layer in the vicinity of the leading edge, with the thickness much smaller than the spanwise separation associated with the freestream disturbances. In this region, the disturbances are governed by the linearized boundary region equations, and the diffusion in the spanwise direction

is in the same order of magnitude as that in the wall-normal direction.

- Region III is the viscous region that follows in the downstream of region II; here, the boundary layer thickness is in the same order of magnitude as the spanwise separation. The flow is governed by the boundary-region equations, which are obtained from the full Navier-Stokes equations by neglecting the streamwise pressure-gradient and the streamwise viscous diffusion.
- Region IV is above region III, and the flow is assumed again inviscid since the viscous effects are negligible. In this region, the flow is influenced at leading order by the displacement effect due to the increased thickness of the viscous layer underneath.

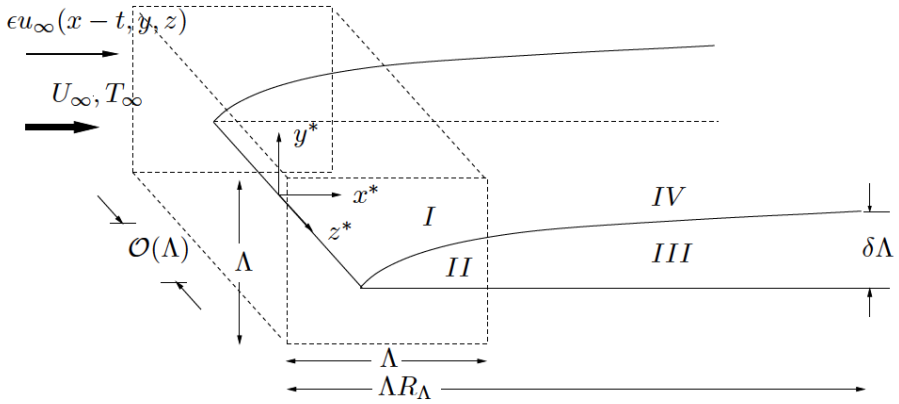

Figure 1. Fhe flow domains illustrating the asymptotic structure (Leib et al.[18]).

The focus in this paper is on region III, where the streamwise wavenumber of disturbances are expected to be small and the flow is governed by the compressible boundary region equations.

A. Scalings

All dimensional spatial coordinates (x^*, y^*, z^*) are normalized by the spanwise separation λ^* of the disturbances, while the dependent variables by their respective freestream values. The pressure field is normalized by the dynamic pressure as follows

$$\bar{t} = \frac{t^*}{\lambda^*/V_\infty^*}; \quad \bar{x} = \frac{x^*}{\lambda^*}; \quad \bar{y} = \frac{y^*}{\lambda^*}; \quad \bar{z} = \frac{z^*}{\lambda^*} \tag{1}$$

$$\bar{u} = \frac{u^*}{V_\infty^*}; \quad \bar{v} = \frac{v^*}{V_\infty^*}; \quad \bar{w} = \frac{w^*}{V_\infty^*}; \quad \bar{\rho} = \frac{\rho^*}{\rho_\infty^*} \tag{2}$$

$$\bar{p} = \frac{p^* - p_\infty^*}{\rho_\infty^* V_\infty^{*2}}; \quad \bar{T} = \frac{T^*}{T_\infty^*}; \quad \bar{\mu} = \frac{\mu^*}{\mu_\infty^*}; \quad \bar{k} = \frac{k^*}{k_\infty^*} \tag{3}$$

where λ^* is the spanwise wavelength of the disturbances, (u^*, v^*, w^*) are the velocity components, ρ^* the density, p^* is pressure, T^* temperature, μ^* dynamic viscosity, k^* thermal conductivity and all quantities with ∞ at the subscript represent conditions at infinity.

Reynolds number based on the spanwise separation, Mach number and Prandtl number are defined as

$$R_\lambda = \frac{\rho_\infty^* V_\infty^* \lambda^*}{\mu_\infty^*}, \qquad Ma = \frac{V_\infty^*}{a_\infty^*}, \qquad Pr = \frac{\mu_\infty^* C_p}{k_\infty^*} \tag{4}$$

where μ^*_∞, a^*_∞ and k^*_∞ are freestream dynamic viscosity, speed of sound and thermal conductivity, respectively, and C_p is the specific heat at constant pressure. For boundary layer flows over curved surfaces, we define the global Görtler number as

$$G_\lambda = \frac{R^2_\lambda \lambda^*}{r^*} \tag{5}$$

where r^* is the radius of the curvature.

B. Boundary-region equations

For a full compressible flow, the primitive form of the Navier-Stokes equations in non-dimensional variables are considered here in the form

$$\frac{D\bar{\rho}}{D\bar{t}} + \rho\left(\frac{\partial \bar{u}}{\partial \bar{x}} + \frac{\partial \bar{v}}{\partial \bar{y}} + \frac{\partial \bar{w}}{\partial \bar{z}}\right) = 0 \tag{6}$$

$$\bar{\rho}\frac{D\bar{u}}{D\bar{t}} = -\frac{\partial \bar{p}}{\partial \bar{x}} + \frac{1}{Re_\lambda}\frac{\partial}{\partial \bar{x}}\left[\frac{2}{3}\mu\left(2\frac{\partial \bar{u}}{\partial \bar{x}} - \frac{\partial \bar{v}}{\partial \bar{y}} - \frac{\partial \bar{w}}{\partial \bar{z}}\right)\right] + \frac{\partial}{\partial \bar{y}}\left[\mu\left(\frac{\partial \bar{u}}{\partial \bar{y}} + \frac{\partial \bar{v}}{\partial \bar{x}}\right)\right] + \frac{\partial}{\partial \bar{z}}\left[\mu\left(\frac{\partial \bar{w}}{\partial \bar{x}} + \frac{\partial \bar{u}}{\partial \bar{z}}\right)\right] \tag{7}$$

$$\bar{\rho}\frac{D\bar{v}}{D\bar{t}} = -\frac{\partial \bar{p}}{\partial \bar{y}} + \frac{1}{Re_\lambda}\frac{\partial}{\partial \bar{y}}\left[\frac{2}{3}\mu\left(2\frac{\partial \bar{v}}{\partial \bar{y}} - \frac{\partial \bar{u}}{\partial \bar{x}} - \frac{\partial \bar{w}}{\partial \bar{z}}\right)\right] + \frac{\partial}{\partial \bar{x}}\left[\mu\left(\frac{\partial \bar{v}}{\partial \bar{x}} + \frac{\partial \bar{u}}{\partial \bar{y}}\right)\right] + \frac{\partial}{\partial \bar{z}}\left[\mu\left(\frac{\partial \bar{v}}{\partial \bar{z}} + \frac{\partial \bar{w}}{\partial \bar{y}}\right)\right] \tag{8}$$

$$\bar{\rho}\frac{D\bar{w}}{D\bar{t}} = -\frac{\partial \bar{p}}{\partial \bar{z}} + \frac{1}{Re_\lambda}\frac{\partial}{\partial \bar{z}}\left[\frac{2}{3}\mu\left(2\frac{\partial \bar{w}}{\partial \bar{z}} - \frac{\partial \bar{u}}{\partial \bar{x}} - \frac{\partial \bar{v}}{\partial \bar{y}}\right)\right] + \frac{\partial}{\partial \bar{x}}\left[\mu\left(\frac{\partial \bar{w}}{\partial \bar{x}} + \frac{\partial \bar{u}}{\partial \bar{z}}\right)\right] + \frac{\partial}{\partial \bar{y}}\left[\mu\left(\frac{\partial \bar{v}}{\partial \bar{z}} + \frac{\partial \bar{w}}{\partial \bar{y}}\right)\right] \tag{9}$$

$$\begin{aligned}
&\bar{\rho}\frac{D\bar{T}}{D\bar{t}} = \frac{1}{PrRe_\lambda}\left[\frac{\partial}{\partial \bar{x}}\left(k\frac{\partial \bar{T}}{\partial \bar{x}}\right) + \frac{\partial}{\partial \bar{y}}\left(k\frac{\partial \bar{T}}{\partial \bar{y}}\right) + \frac{\partial}{\partial \bar{z}}\left(k\frac{\partial \bar{T}}{\partial \bar{z}}\right)\right] \\
-\ &(\gamma-1)M^2_\infty\left[p\left(\frac{\partial \bar{u}}{\partial \bar{x}} + \frac{\partial \bar{v}}{\partial \bar{y}} + \frac{\partial \bar{w}}{\partial \bar{z}}\right) - \frac{2}{3}\mu\left(\frac{\partial \bar{u}}{\partial \bar{x}} + \frac{\partial \bar{v}}{\partial \bar{y}} + \frac{\partial \bar{w}}{\partial \bar{z}}\right)^2\right] \\
+\ &(\gamma-1)M^2_\infty\frac{\mu}{Re_\lambda}\left[2\left(\frac{\partial \bar{u}}{\partial \bar{x}}\right)^2 + 2\left(\frac{\partial \bar{v}}{\partial \bar{y}}\right)^2 + 2\left(\frac{\partial \bar{w}}{\partial \bar{z}}\right)^2 + \left(\frac{\partial \bar{u}}{\partial \bar{y}} + \frac{\partial \bar{v}}{\partial \bar{x}}\right)^2 + \left(\frac{\partial \bar{w}}{\partial \bar{x}} + \frac{\partial \bar{u}}{\partial \bar{z}}\right)^2 + \left(\frac{\partial \bar{v}}{\partial \bar{z}} + \frac{\partial \bar{w}}{\partial \bar{y}}\right)^2\right]
\end{aligned} \tag{10}$$

where

$$\frac{D}{D\bar{t}} = \frac{\partial}{\partial \bar{t}} + \bar{u}\frac{\partial}{\partial \bar{x}} + \bar{v}\frac{\partial}{\partial \bar{y}} + \bar{w}\frac{\partial}{\partial \bar{z}} \tag{11}$$

is the substantial derivative. The pressure p, the temperature T and the density of the fluid are combined in the equation of state in non-dimensional form, $\bar{p} = \bar{\rho}\bar{T}/\gamma M^2_\infty$, assuming that non-chemically-reacting flows are considered. Other notations include the dynamic viscosity μ, Reynolds number $Re = \rho_\infty V^*_\infty \lambda^*/\mu$ based on a characteristic velocity V^*_∞, and the spanwise separation λ^*, and the free-stream Mach number $M_\infty = V^*_\infty/a^*_\infty$. The dynamic viscosity and thermal conductivity k is linked to the temperature using the power law in dimensionless form,

$$\mu = T^b; \qquad k = \frac{C_p \mu}{Pr} \tag{12}$$

where $b = 0.76$, $C_p = \gamma R/(\gamma - 1)$, $\gamma = 1.4$, and $Pr = 0.72$ for air.

Region III is where $x/R_\lambda = O(1)$, which implies that the streamwise ellipticity is weak and negligible (see Ricco & Wu,[29] Ricco,[28] or Marensi et al.[24]). The compressible boundary region equations can be derived from the full compressible Navier-Stokes equations. Based in the above assumption, the streamwise distance can be scaled as $x = \bar{x}/R_\lambda$ while the other two are the same $y = \bar{y}$, $z = \bar{z}$, and the time as $t = \bar{t}/R_\lambda$. Also, the crossflow components of velocity are expected to be small compared to the streamwise component, and variations of pressure are expected to be small. This suggest the introduction of the scaling of dependent variables as:

$$u = \bar{u}; \quad v = \bar{v}/R_\lambda; \quad w = \bar{w}/R_\lambda; \quad \rho = \bar{\rho}; \quad p = \bar{p}/R_\lambda^2; \quad T = \bar{T}; \quad \mu = \bar{\mu}; \quad k = \bar{k}; \tag{13}$$

Inserting (24) into the full Navier-Stokes equations, and performing on order-of-magnitude analysis, the nonlinear compressible boundary region equations are obtained in the form

$$\begin{aligned}
&\frac{D\rho}{Dt} + \rho\nabla\cdot\vec{V} = 0 \\
&\rho\frac{Du}{Dt} = \nabla_c\cdot(\mu\nabla_c u) \\
&\rho\frac{Dv}{Dt} = -\frac{\partial p}{\partial y} + \frac{\partial}{\partial y}\left[\frac{2}{3}\mu\left(3\frac{\partial v}{\partial y} - \nabla\cdot\vec{V}\right)\right] + \frac{\partial}{\partial x}\left(\mu\frac{\partial u}{\partial y}\right) + \frac{\partial}{\partial z}\left[\mu\left(\frac{\partial v}{\partial z} + \frac{\partial w}{\partial y}\right)\right] - G_\lambda u^2 \\
&\rho\frac{Dw}{Dt} = -\frac{\partial p}{\partial z} + \frac{\partial}{\partial z}\left[\frac{2}{3}\mu\left(3\frac{\partial w}{\partial z} - \nabla\cdot\vec{V}\right)\right] + \frac{\partial}{\partial x}\left(\mu\frac{\partial u}{\partial z}\right) + \frac{\partial}{\partial y}\left[\mu\left(\frac{\partial v}{\partial z} + \frac{\partial w}{\partial y}\right)\right] \\
&\rho\frac{DT}{Dt} = \frac{1}{Pr}\nabla_c\cdot(k\nabla_c T) + (\gamma-1)M_\infty^2\mu\left[\left(\frac{\partial u}{\partial y}\right)^2 + \left(\frac{\partial u}{\partial z}\right)^2\right]
\end{aligned} \tag{14}$$

where ∇_c is the crossflow nabla operator:

$$\nabla_c = \frac{\partial}{\partial y}\vec{j} + \frac{\partial}{\partial z}\vec{k} \tag{15}$$

and $G_\lambda u^2$ is the term that accounts for the curvature.

This set of equations is parabolic in the streamwise direction and elliptic in the spanwise direction. Appropriate initial/upstream and boundary conditions are necessary to close the problem; these conditions are the same as those used by Ricco & Wu[29] (see also Ricco[28]).

$$\begin{aligned}
&u = 2xU_0 + (2x)^{3/2}U_1 \\
&v = V_0 + (2x)^{1/2}V_1 + \frac{i}{(\kappa_2 - i|\kappa|)(2x)^{1/2}}\left[e^{i\kappa_2(2x)^{1/2}\eta - (\kappa^2+\kappa_2^2)x} - e^{-|\kappa|(2x)^{1/2}\eta}\right] \\
&- \left[V_c - \frac{1}{2}g_1|\kappa|(2x)^{1/2}\right]e^{-|\kappa|(2x)^{1/2}\eta} - v_c \\
&w = W_0 + (2x)^{1/2}W_1 + \frac{i}{\kappa_2 - i|\kappa|}\kappa_2\left[e^{i\kappa_2(2x)^{1/2}\eta - (\kappa^2+\kappa_2^2)x} - i|\kappa|e^{-|\kappa|(2x)^{1/2}\eta}\right] \\
&- V_c|\kappa|(2x)^{1/2}e^{-|\kappa|(2x)^{1/2}\eta} - w_c \\
&T = 2xT_0 + (2x)^{3/2}T_1 \\
&p = \frac{P_0}{(2x)^{1/2}} + P_1 + \left[g_1 - \frac{V_c}{|\kappa|(2x)^{1/2}}\right]e^{-|\kappa|(2x)^{1/2}\eta} - p_c
\end{aligned} \tag{16}$$

where $\kappa_2 = \frac{k_2}{(k_1 Re_\lambda)^{1/2}}$, $\kappa = \frac{k_3}{(k_1 Re_\lambda)^{1/2}}$, and (k_1, k_2, k_3) are the components of the wavenumber vector of the disturbance. The equations for U_n, V_n, W_n, T_n, and P_n, $n = 1, 2$, as well as for V_c, g_1, v_c, w_c and p_c are given in Appendix D of Ricco 2007. For small amplitude disturbances we can use the conditions for velocity and pressure from the incompressible boundary region equations (Goldstein et al.[6] or Sescu & Thompson[35])

The nonlinear compressible boundary equations were numerically solved using an algorithm similar to the one used in Sescu & Thompson,[35] but adapted to the compressible regime.

III. Results and Discussion

Numerical simulations of the nonlinear boundary region equations (14), for Mach number ranging from 0.8 and 6, are carried out. Since there are no obstructions in the flow no shock waves are generated (this has been previously considered in several studies; see, for example, Li et al.[20] or Ren & Fu[27]), while the mean inflow condition is generated from the similarity solution, which is obtained by means of the Dorodnitsyn-Howarth coordinate transformation

$$\bar{Y}(x,y) = \int_0^y \rho(x,\tilde{y})d\tilde{y} \tag{17}$$

A similarity variable is defined as

$$\eta = \bar{Y}\left(\frac{Re_x}{2x}\right)^{1/2}, \tag{18}$$

where Re_x is the Reynolds number based on the distance from the leading edge, and the base velocity and temperature can be expressed as

$$U = F'(\eta), \quad V = (2xRe_x)^{-1/2}(\eta_c T F' - TF), \quad T = T(\eta) \tag{19}$$

where prime represents differentiation with respect to η, and $\eta_c = 1/T\int_0^\eta T(\tilde{\eta})d\tilde{\eta}$. F and T satisfy the following coupled equations

$$\begin{aligned} &\left(\frac{\mu}{T}F''\right)' + FF'' = 0, \\ &\frac{1}{Pr}\left(\frac{\mu}{T}T'\right)' + FT' + (\gamma-1)M^2\frac{\mu}{T}F''^2 = 0, \end{aligned} \tag{20}$$

satisfying the boundary conditions

$$F(0) = F'(0) = 0, \quad T'(0) = 0, \quad F' \to 1, \quad T \to 1 \to as \to \eta \to \infty \tag{21}$$

The dependence of the viscosity on the temperature is assumed to be described by the power law,

$$\mu = T^b, \quad b = 0.76 \tag{22}$$

Equations (20) were solved by a shooting method for both adiabatic and isothermal conditions. Figure 2 shows this solution for Mach number equal to 3, and for both isothermal and adiabatic wall conditions.

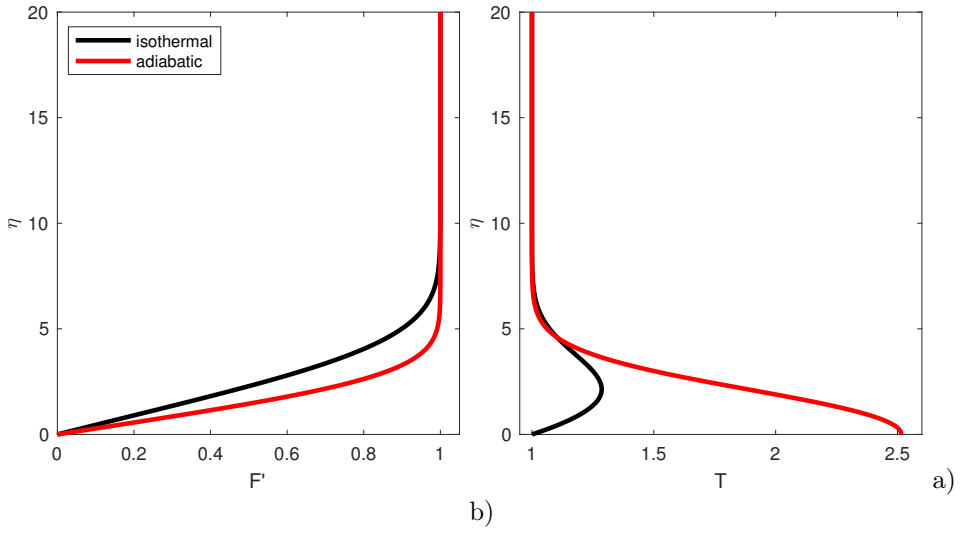

Figure 2. Base flow solution.

Figure 3 shows a sketch of the flow domain, where the region III is in blue.

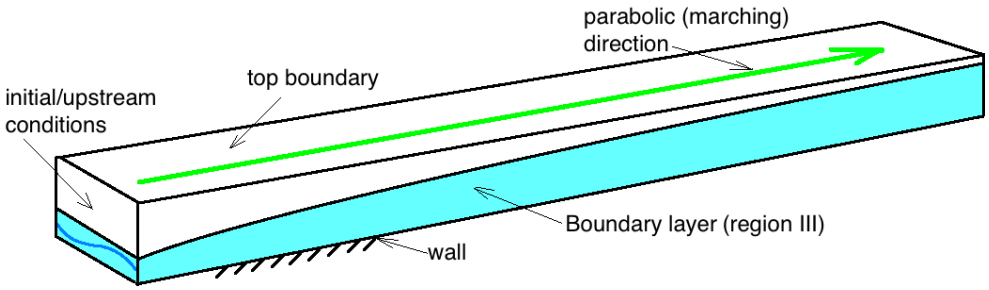

Figure 3. Flow domain.

Gortler vortices are excited by a small disturbance imposed on the base flow at the inflow boundary. The Mach number is varied from a high-subsonic value ($M = 0.8$) to a low hypersonic value ($M = 6.0$), while the spanwise separation is varied between 0.3 cm to 0.6 cm. The Reynolds number based on the distance from the leading edge, used to calculate the similarity solution that is imposed at the upstream boundary, is maintained constant for all cases (of course, this implies that the Reynolds number based on the spanwise separation is not the same). The radius of curvature of the concave surface is 2 m far all cases.

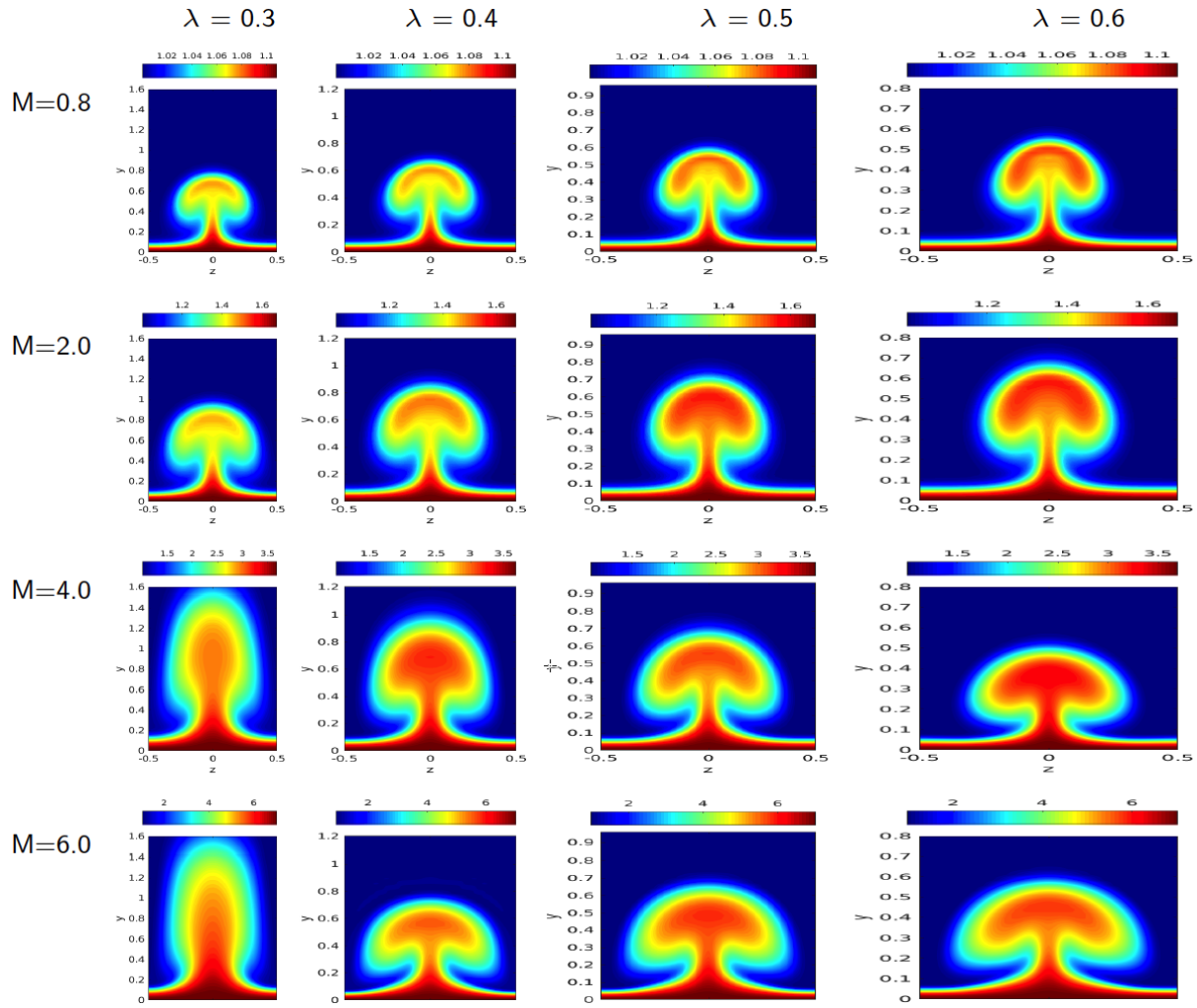

Figure 4. Contour plots of temperature in crossflow planes for different Mach numbers and spanwise separations (adiabatic wall condition).

In figures 4 and 5, we show contour plots of temperature in a certain cross-stream plane (right after the energy saturation point), for all Mach numbers and spanwise separations, where the same disturbances amplitude (relative to the free stream velocity) has been imposed at the inflow boundary. Figure 4 corresponds to the adiabatic wall condition, where it is noticed that there is a high increase of the wall temperature, especially for the highest Mach number. The variation of the spanwise separation is along the horizontal direction, while Mach number is varied along the vertical direction. Looking at the smallest Mach number, $M = 0.8$, in the first row of figure 4, it can be observed that as the spanwise separation is increased the mushroom shapes becomes smaller relative to the spanwise separation (the distance between the mushroom shapes increases). Looking at the last row of contour plots in figure 4, we noticed that as the spanwise separation is increased the mushroom shapes are fuller and less localized. The mushroom shapes corresponding to the isothermal wall condition in figure 5 has altered the morphology in that for the highest Mach number the vortices are more localized; in fact, the contours of all Mach numbers seem to have the same spanwise separation. This would suggest that the high increase of the temperature in proximity to the wall (under adiabatic condition) makes the mushroom shapes fuller.

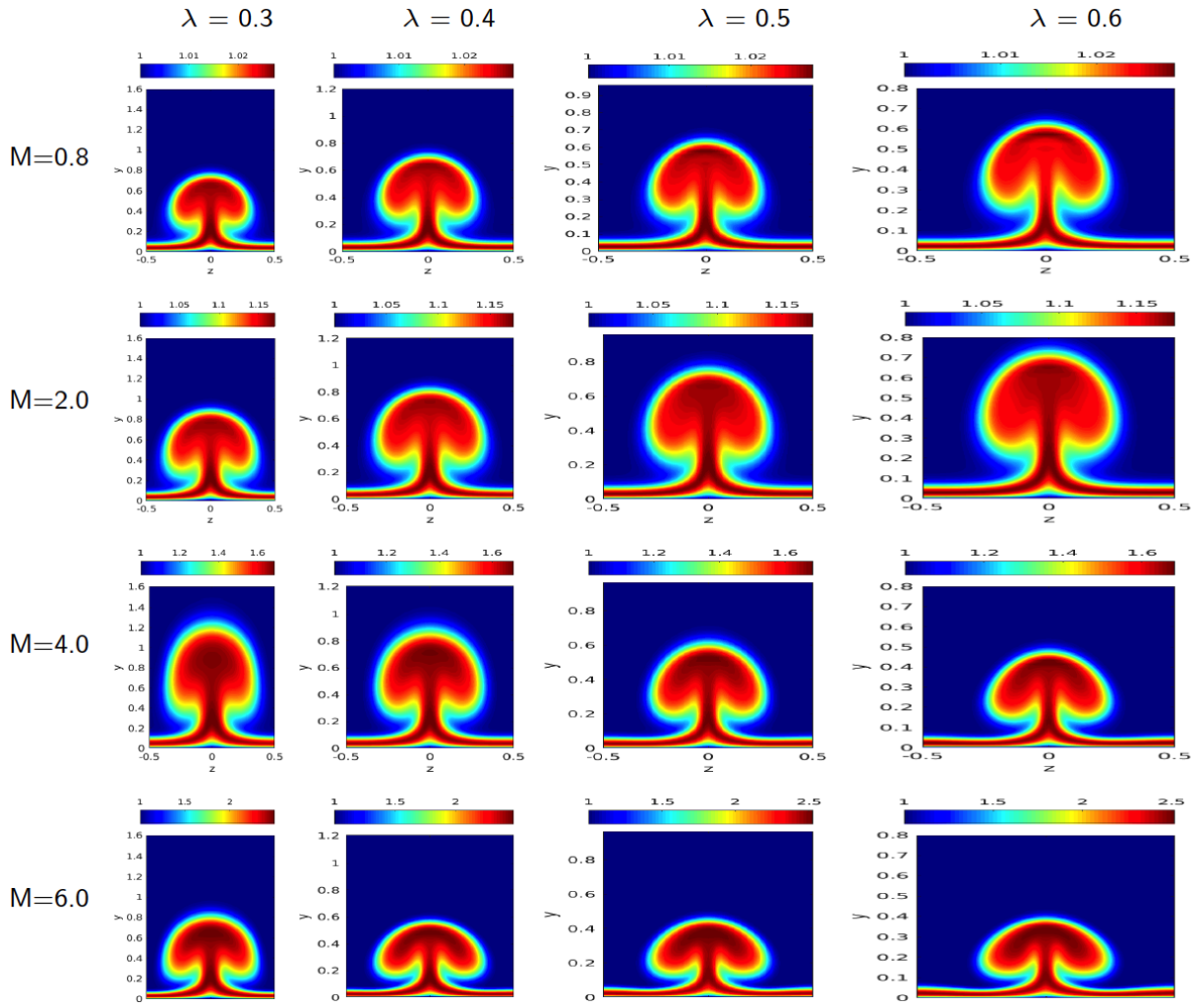

Figure 5. Contour plots of temperature in crossflow planes for different Mach numbers and spanwise separations (isothermal wall condition).

We quantify the vortex energy as

$$E(x) = \int_{z_1}^{z_2} \int_{0}^{\infty} \left[|u(x,y,z) - u_m(x,y)|^2 + |v(x,y,z) - v_m(x,y)|^2 + |w(x,y,z) - w_m(x,y)|^2 \right] dzdy, \qquad (23)$$

where $u_m(x,y)$, $v_m(x,y)$, and $w_m(x,y)$ are the spanwise mean components of velocity, and z_1 and z_2 are the coordinates of the boundaries in the spanwise direction.

In figure 6, the vortex energy distribution versus the streamwise coordinate x is plotted for all spanwise separation and Mach numbers. A reduction of the scaled energy is obtained as the spanwise separation is increased for both the isothermal (in black) and adiabatic (in red) wall conditions, and for all Mach numbers; the energy saturation location moves downstream as the spanwise separation is increased. The energy level corresponding to the adiabatic condition is slightly lower for the smallest Mach number (figure 6a), but it becomes higher as the Mach number is increased, while the saturation location moves further downstream.

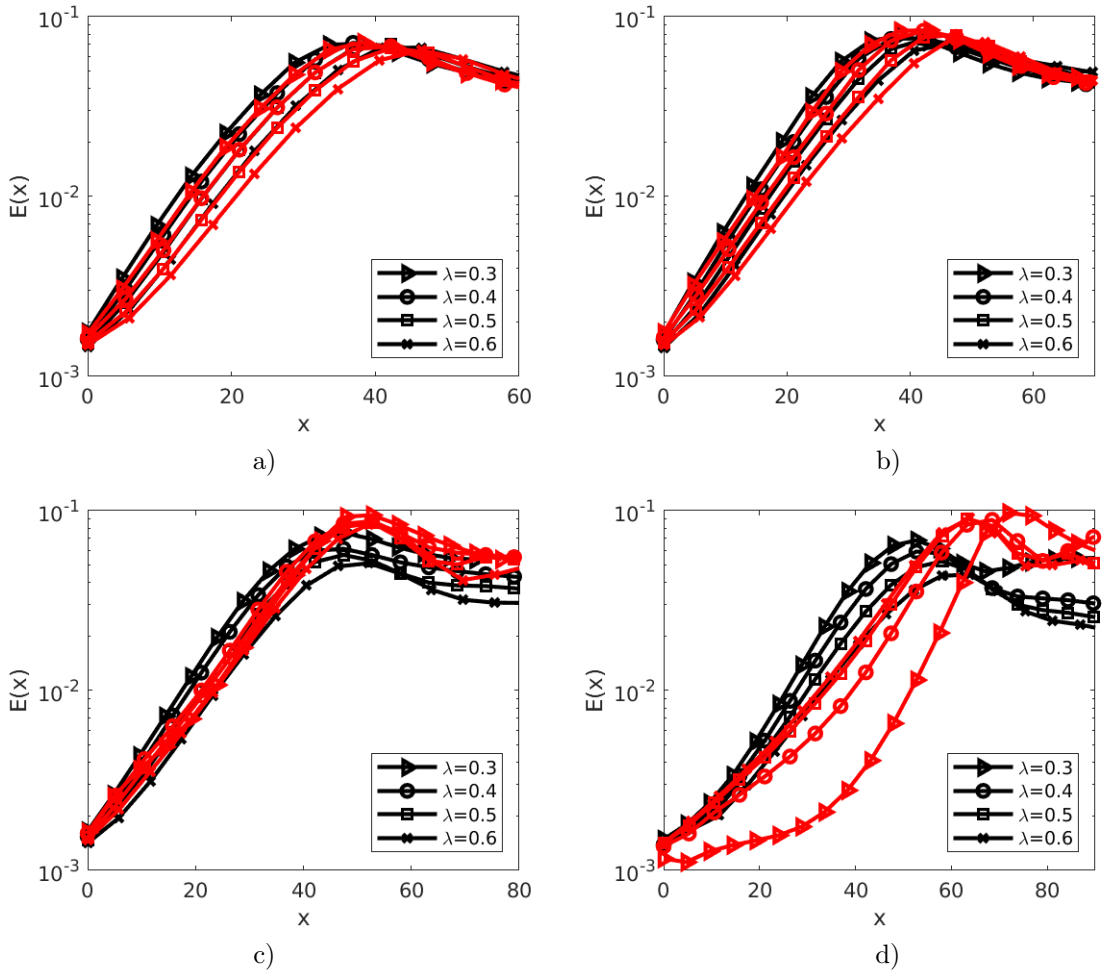

Figure 6. Vortex energy distribution along the streamwise direction: a) $M = 0.8$**; a)** $M = 2.0$**; a)** $M = 4.0$**; a)** $M = 6.0$**.**

The spanwise averaged wall shear stress is calculated according to

$$\tau_w(x) = \frac{1}{(z_2 - z_1)} \int_{z_1}^{z_2} \left. \frac{\partial u}{\partial y} \right|_{y=0} (x, 0, z) dz, \tag{24}$$

where we take the derivative of the streamwise velocity with respect to the wall-normal direction at the wall. In figure 7, the spanwise averaged wall shear stress is plotted against the streamwise coordinate in both isothermal and adiabatic conditions. In all cases, the wall shear stress increases as the spanwise separation increases, and - as expected - the wall shear stress is smaller for the adiabatic condition, as a result of the high level of heating in proximity to the wall. There is also an jump of the wall shear stress approximately at the streamwise location corresponding to the energy saturation initiation.

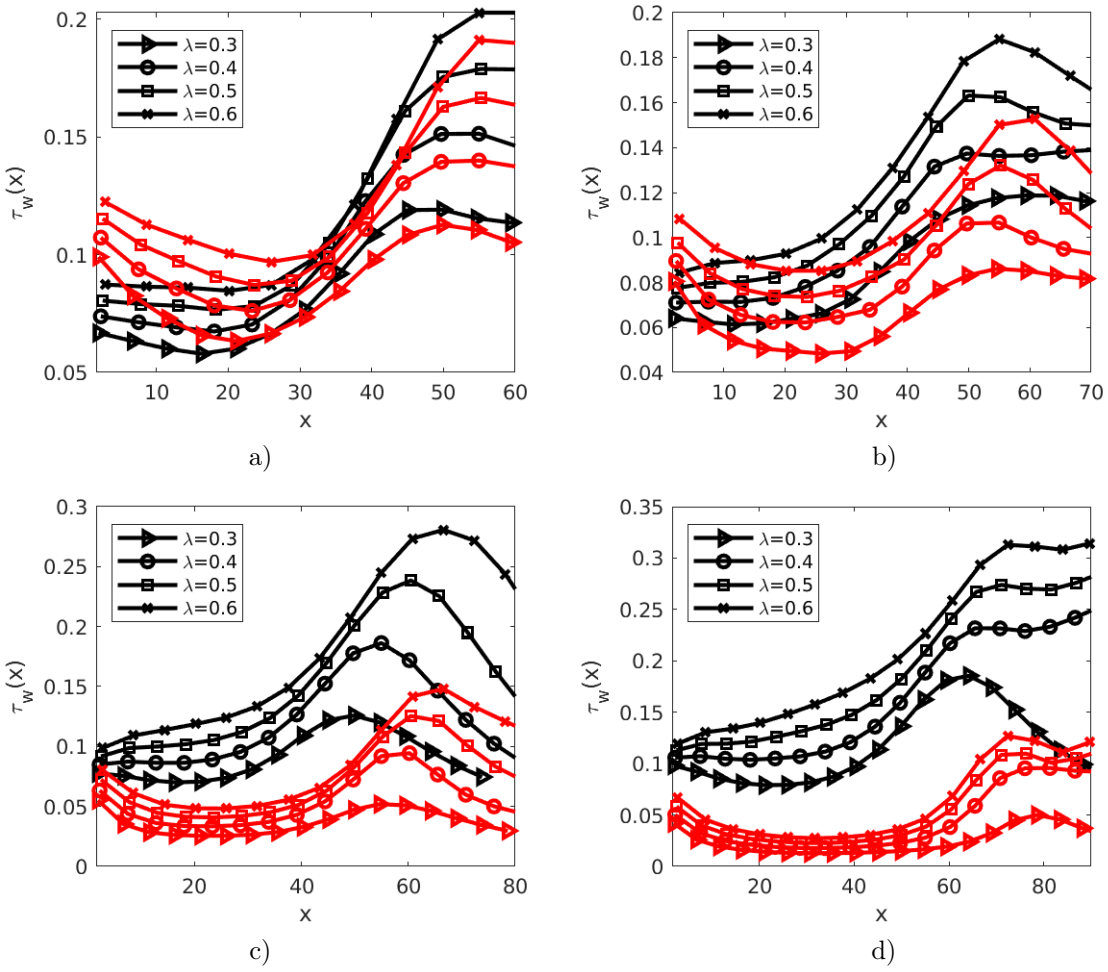

Figure 7. Spanwise averaged wall shear stress distribution along the streamwise direction: a) $M = 0.8$**; a)** $M = 2.0$**; a)** $M = 4.0$**; a)** $M = 6.0$**.**

Finally, we quantify the spanwise averaged wall heat flux according to

$$q_w(x) = -\frac{1}{(z_2 - z_1)} \int_{z_1}^{z_2} \left. \frac{\partial T}{\partial y} \right|_{y=0} (x, 0, z) dz. \tag{25}$$

The results for the isothermal wall (note that under the adiabatic wall condition the wall heat flux is zero) are included in figure 8. The wall heat flux shows a decrease as the spanwise separation is increased; there is also a decay of the wall heat flux in the streamwise coordinate range where the energy saturation occurs.

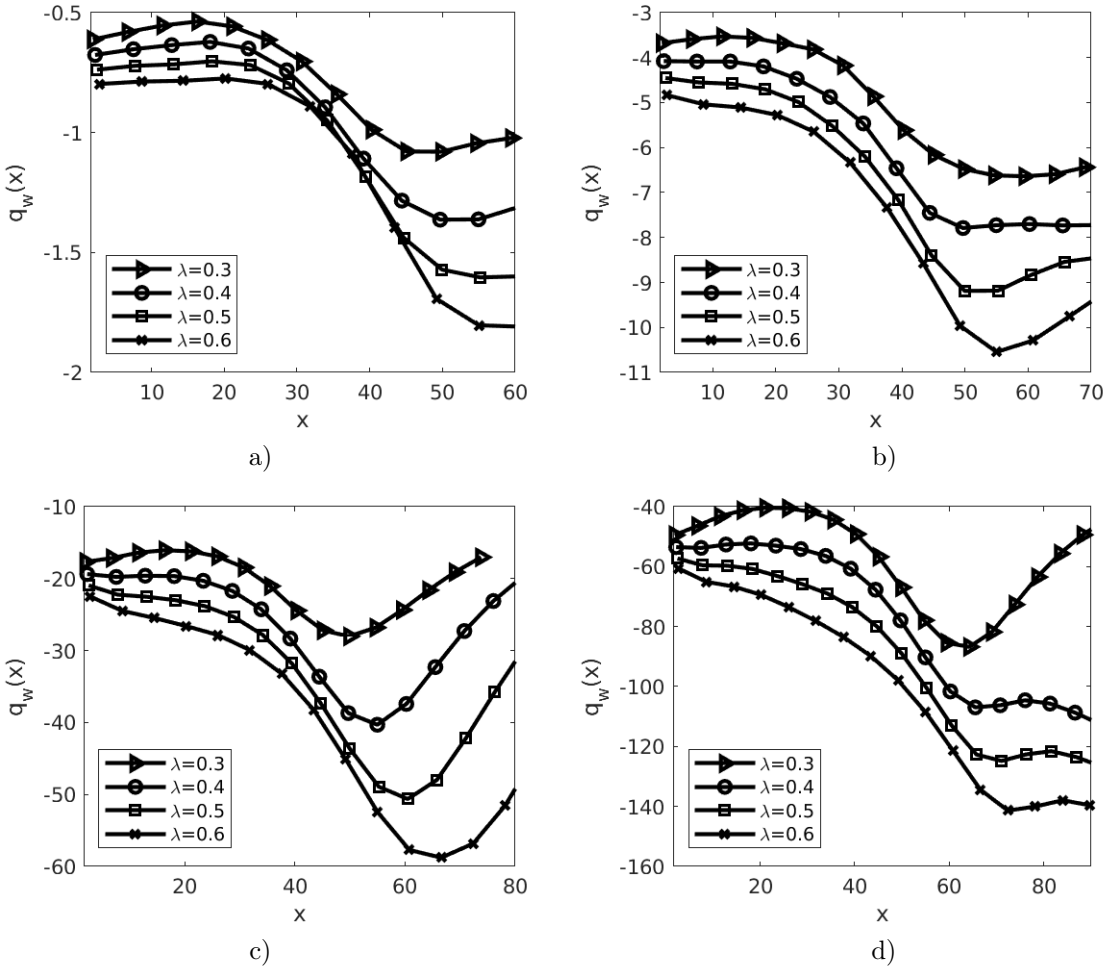

Figure 8. Spanwise averaged wall heat flux distribution along the streamwise direction: a) $M = 0.8$**; a)** $M = 2.0$**; a)** $M = 4.0$**; a)** $M = 6.0$**.**

IV. Conclusions

We studied Gortler vortices that develop in high-speed boundary layer flows over concave surfaces, by using the numerical solution to the compressible nonlinear boundary region equations. We targeted the nonlinear development of these centrifugal instabilities, by varying the spanwise separation that characterizes the upstream disturbance (and dictate the spanwise separation of the downstream Gortler vortices) and the Mach number.

A range of spanwise separations was considered, and the Mach number covered a high-subsonic, two supersonic, and a low-hypersonic cases. Contours of temperature in crossflow planes at a certain streamwise location showed that, for the smallest Mach number, $M = 0.8$, in the adiabatic condition, as the spanwise separation is increased and that the mushroom shapes become smaller relative to the spanwise separation (the distance between the mushroom shapes increases). For the highest Mach number, as the spanwise separation was increased the mushroom shapes become fuller and less localized. The mushroom shapes corresponding to the isothermal wall condition in figure 5 showed that for the highest Mach number the vortices are more localized.

The kinetic energy of the instabilities was calculated an plotted against the streamwise coordinate. It was observed that as the spanwise separation is increased, the scaled kinetic energy maximum increases, and that the streamwise location, where the energy saturation sets in, moves downstream as the spanwise separation is increased. We also calculated the wall shear stress and the wall heat flux, and observed that the

wall shear stress increases as the spanwise separation increases, and - as expected - the wall shear stress is smaller for the adiabatic condition, as a result of the high level of heating in proximity to the wall. There was also an jump of the wall shear stress approximately at the streamwise location corresponding to the energy saturation initiation. The results in terms of the wall heat flux for the isothermal wall showed a decrease as the spanwise separation is increased; there was also a decay of the wall heat flux in at the streamwise location corresponding to where the energy saturation is initiated.

References

[1]Boiko, A.V., Ivanov, A.V., Kachanov, Y.S. and Mischenko, D.A. (2010) Steady and unsteady Görtler boundary-layer instability on concave wall, *European Journal of Mechanics B/Fluids*, Vol. 29, pp. 61-83.

[2]Choudhari, M. and Fischer, P. (2005) Roughness induced Transient Growth, *AIAA Paper 2005-4765*.

[3]Depmsey, L.D., Hall, P. & Deguchiu, K. (2017) The excitation of Gortler vortices by free stream coherent structures, *J. Fluid Mech.*, Vol. 826, pp. 60-96.

[4]Dryden, H. L. (1955) Transition from laminar to turbulent flow at subsonic and supersonic speeds. Conference on High-Speed Aeronautics, 41, Polytechnic of Brooklyn, New York.

[5]Fedorov, A.V. (2015) Prediction and control of laminar-turbulent transition in high-speed boundary layers, Procedia IUTAM, Vol. 14, pp. 3-14.

[6]Goldstein, M., Sescu, A., Duck, P. and Choudhari, M. (2010) The Long Range Persistence of Wakes behind a Row of Roughness Elements, *Journal of Fluid Mechanics*, Vol. 644, pp. 123-163.

[7]Goldstein, M., Sescu, A., Duck, P. and Choudhari, M. (2011) Algebraic/transcendental Disturbance Growth behind a Row of Roughness Elements, *Journal of Fluid Mechanics*, Vol. 668, pp. 236-266.

[8]Goldstein, M., Sescu, A., Duck, P. and Choudhari, M. (2016) Nonlinear wakes behind a row of elongated roughness elements, *Journal of Fluid Mechanics*, Vol. 796, pp. 516-557.

[9]Goldstein, M. & Sescu (2008) Boundary-layer transition at high free-stream disturbance levels - beyond Klebanoff modes. *J. Fluid Mech.*, Vol. 613, pp. 95-124.

[10]Görtler, H . (1941) Instabilita-umt laminarer Grenzchichten an Konkaven Wanden gegenber gewissen dreidimensionalen Storungen, *ZAMM*, Vol. 21, pp. 250–52; english version: *NACA Report 1375* (1954)

[11]Gregory, N. and Walker, W.S. (1950) The effect on transition of isolated surface excrescences in the boundary-layer ıARC Technical Report 13, pp. 436; published as Aeronaut. Res. Council R&M 2779 (1956), pp. 1-10.

[12]Hall, P. (1982) Taylor-Görtler vortices in fully developed or boundary-layer flows: linear theory, *Journal of Fluid Mechanics*, Vol. 124, pp. 475-494.

[13]Hall, P. (1983) The linear development of Görtler vortices in growing boundary layers, *Journal of Fluid Mechanics*, Vol. 130, pp. 41-58.

[14]Hall, P. and Horseman. N. (1991) The linear inviscid secondary instability of longitudinal vortex structures in boundary layers. *Journal of Fluid Mechanics*. Vol. 232, pp. 357-375.

[15]Kendall, J. (1975) Wind tunnel experiments relating to supersonic and hypersonic boundary layer transition. *AIAA J.* 13, 290Ð299.

[16]Kendall, J.M. (1998) Experiments on boundary-layer receptivity to freestream turbulence. *AIAA Paper 2004-2335*.

[17]Landahl, M.T. (1980) A note on an algebraic instability of inviscid parallel shear flows. *J. Fluid Mech.*, Vol. 98, pp. 243-251.

[18]Leib, S.J., Wundrow, W. & Goldstein, M. (1999) Effect of free-stream turbulence and other vortical disturbances on a laminar boundary layer. *J. Fluid Mech.*, Vol. 380, pp. 169-203.

[19]Li, F. and Malik, M. (1995) Fundamental and subharmonic secondary instabilities of Görtler vortices, *Journal of Fluid Mechanics*, Vol. 297, pp. 77-100.

[20]Li, F., Choudhari, M., Chang, C.-L., Greene, P., and Wu, M. (2010) Development and Breakdown of Gortler Vortices in High Speed Boundary Layers", 48th AIAA Aerospace Sciences Meeting Including the New Horizons Forum and Aerospace Exposition, Aerospace Sciences Meetings.

[21]Liu. X., Osher, S. and Chan, T. (1994) Weighted essentially non-oscillatory schemes, Journal of Computational Physics, Vol. 115, pp. 200-212.

[22]Mack, L. (1975) Linear stability theory and the problem of supersonic boundary layer transition. *AIAA J.* 3, 278Ð289.

[23]Malik, M.R. & Hussaini, M.Y. (1990) Numerical simulation of interactions between Gortler vortices and Tollmien-Schlichting waves. *J. Fluid Mech.*, Vol. 210, pp. 183-199.

[24]Marensi, E., Ricco, P. & Wu, X. (2017) Nonlinear unsteady streaks engendered by the interaction of free-stream vorticity with a compressible boundary layer. *J. Fluid Mech.*. Vol. 817, pp. 80-121.

[25]Matsubara, M. and Alfredsson, P.H. (2001) Disturbance growth in boundary layers subjected to free stream turbulence, *J. Fluid Mech.*, Vol. 430, pp. 149.

[26]Pate, S. R. (1971) Supersonic boundary-layer transition: effects of roughness and free-stream disturbances. *AIAA J.* 9, 797-803.

[27]Ren, J. & Fu, S. (2017) Secondary instabilities of Gortler vortices in high-speed boundary layer flows, *J. Fluid Mech.*, Vol. 781, pp. 388-421.

[28]Ricco, P. (2006) Response of a compressible laminar boundary layer to free-stream turbulence. PhD thesis, University of London.

[29]Ricco, P. & Wu, X. 2007 Response of a compressible laminar boundary layer to free-stream vortical disturbances, *J. Fluid Mech.*, Vol. 587, pp. 97-138.

[30]Ricco, P., Shah, D. & Hicks, P. D. (2013) Compressible laminar streaks with wall suction. *Phys. Fluids* 25, 054110.

[31]Ricco, P., Tran, D.-L. & Ye, G. (2009) Wall heat transfer effects on Klebanoff modes and Tollmien- Schlichting waves in a compressible boundary layer. *Phys. Fluids* 21, 024106.

[32]Saric, W.S. (1994) Görtler Vortices, *Annu. Rev. Fluid Mech.*, Vol. 26, pp. 379-409.

[33]Sescu, A., Taoudi, L. and Afsar, M. (2017) Iterative control of Görtler vortices via local wall deformations, *Theoretical and Computational Fluids Dynamics*, DOI 10.1007/s00162-017-0440-2.

[34]Sescu, A., Pendyala, R. and Thompson, D. (2014) On the Growth of Görtler Vortices Excited by Distributed Roughness Elements, AIAA Paper 2014-2885.

[35]Sescu, A. and Thompson, D. (2015) On the Excitation of Görtler Vortices by Distributed Roughness Elements, *Theoretical and Computational Fluids Dynamics*, Vol. 29, pp. 67-92.

[36]Schneider, S. P. (2001) Effect of high-speed tunnel noise on laminar-turbulent transition. *J. Sp. Rock.* 38-3, 323-333.

[37]Swearingen, J.D. and Blackwelder, R.F. (1987) The growth and breakdown of streamwise vortices in the presence of a wall. *J. Fluid Mech.*, Vol. 182, pp. 255-290.

[38]Tam, C.K.W. and Webb, J.C. (1993), Dispersion-relation-preserving finite difference schemes for Computational Aeroacoustics, *Journal of Computational Physics*, Vol. 107, pp. 262-281.

[39]Tani, I. (1962) Production of longitudinal vortices in the boundary-layer along a curved wall, *J. Geophys. Res.*, Vol. 67, pp. 3075.

[40]Westin, K.J.A., Boiko, A.V., Klingmann, B.J.B., Kozlov, V.V. & Alfredsson, P.H. (1994) Experiments in a boundary layer subjected to free stream turbulence. part 1. Boundary layer structure and receptivity. *J. Fluid Mech.*, Vol. 281, pp. 193-218.

[41]White, E.B. (2002) Transient growth of stationary disturbances in a flat plate boundary layer, *Phys. Fluids*, Vol. 14, pp. 4429-4439.

[42]White, E.B., Rice, J.M. and Ergin, F.G. (2005) Receptivity of stationary transient disturbances to surface roughness, *Physics of Fluids*, Vol. 17, pp. 064109.

[43]Wu, X. and Choudhari, M. (2011) Linear and nonlinear instabilities of a blasius boundary layer perturbed by streamwise vortices. Part 2. Intermittent instability induced by long wavelength Klebanoff modes. *J. Fluid Mech.*. Vol. 483, pp. 249-286.

[44]Wu, X, Zhao, D. and Luo, J (2011) Excitation of steady and unsteady Görtler vortices by free-stream vortical disturbances, *Journal of Fluid Mechanics*, Vol. 682, pp. 66-100.

[45]Xu, D., Zhang, Y. & Wu, X. (2017) Nonlinear evolution and secondary instability of steady and unsteady Gortler vortices induced by free-stream vortical disturbances, *J. Fluid Mech.*, Vol. 829, pp. 681-730.

[46]Xu, G., Xiao, Z. & Fu, S. (2011) Secondary instability control of compressible flow by suction for a swept wing, Physics, Mechanics & Astronomy, Vol. 54, pp. 2040-2052.

[47]Zaki, T.A. & Durbin, P. (2005) Mode interaction and the bypass route to transition. *J. Fluid Mech.*, Vol. 531, pp. 85-111.